Two-level atom coupled to a squeezed vacuum inside a coherently driven cavity

Daniel Erenso and Reeta Vyas
Department of Physics, University of Arkansas, Fayetteville, Arkansas 72701
(Received 8 September 2001; published 5 June 2002)

A single two-level atom in a coherently driven cavity and damped by a broadband squeezed vacuum centered about the atomic transition frequency is studied. A second-order Fokker-Planck equation for this system is obtained without using system size expansion. Effects of detunings and cavity decays are also incorporated in the Fokker-Planck equation. This equation is used to study atomic inversion, fluorescent spectrum, and the intensity correlations of the transmitted and fluorescent photons in the bad-cavity limit. Several interesting effects in the atomic inversion, spectrum, and intensity correlations due to the squeezed vacuum are presented. These results are also compared with an atom that is damped by a thermal reservoir.

DOI: 10.1103/PhysRevA.65.063808 PACS number(s): 42.50.Lc, 42.50.Ct, 42.50.Dv, 42.50.Ar

I. INTRODUCTION

With the generation and detection of squeezed light [1–4] increasing attention is being given to the study of interaction of squeezed light with a two-level atom [5–13]. Gardiner studied a single two-level atom embedded in a broadband squeezed vacuum and showed that the two quadratures of the atomic polarization decay at two distinct decay rates that are sensitive to the phase correlations of the squeezed vacuum [5]. Carmichael *et al.* [6] studied the fluorescent spectrum of an atom immersed in a broadband squeezed vacuum when the atom is driven by a coherent field. They predicted that for weak driving fields the incoherent spectrum would narrow as the amount of squeezing is increased. In this limit the spectrum is insensitive to the relative phase between the driving field and the squeezed vacuum. For strong driving fields, on the other hand, the central peak of the Mollow spectrum can broaden or narrow, depending on the relative phase between the squeezed vacuum and the driving field. The photon number distribution for this system has been calculated by Jagatap and Lawande [7]. Vyas and Singh considered resonance fluorescence in the weak-field limit when the atom is driven by squeezed light from an optical parametric oscillator [8], Lyublinskaya and Vyas considered when the atom is driven by nonclassical light from intracavity second harmonic generation and a homodyne degenerate parametric oscillator [9].

Parkins and Gardiner [10] considered a single two-level atom in a cavity when the squeezed light is incident upon one of the output mirrors. Rice and Pedrotti [11] placed a two-level atom coupled to an ordinary vacuum inside a coherently driven optical cavity coupled to a broadband squeezed reservoir through the output mirror. They found that it was possible to overcome the cavity enhancement part of the linewidth. This work was extended by Rice and Baird [12] to calculate the second order intensity correlation function $g^{(2)}(\tau)$ and spectra of the fluorescent light.

In this paper we study a single two-level atom placed inside a coherently driven cavity where the atom is directly coupled to a squeezed vacuum but the cavity mode decays into an ordinary vacuum. The squeezed vacuum spectrum is considered to be broadband centered at the atomic transition frequency. The model proposed here can be implemented by assuming a short cavity, which subtends a large solid angle at the atom. Squeezed modes of the short cavity are directly coupled to the atom. Another cavity with its axis perpendicular to the short cavity is driven by a coherent driving field.

We derive an exact Fokker-Planck equation following the approach of Wang and Vyas [14–16]. An appealing feature of the Fokker-Planck equation approach is that it allows quantum-operator averages to be calculated as classical-like averages. Thus analogies between classical and quantum fluctuations can be drawn that help in developing an intuitive feeling for quantum fluctuations. The Fokker-Planck equation can be converted into a set of stochastic differential equations which can be solved numerically and in many cases analytically. We study the effects of a squeezed vacuum on atomic inversion, the fluorescent spectrum, and the second-order intensity correlation function of the transmitted and fluorescent light in the bad-cavity limit. We find that in the presence of squeezing the threshold value of the cooperativity parameter for seeing vacuum Rabi splitting can be lowered. This behavior is phase sensitive and cannot be seen if squeezed light is replaced by thermal light. We find that the transmitted light can show antibunching even for a large cooperativity parameter. We explain the behavior of antibunching in terms of self-homodying of coherent and incoherent components. We also find that, for large values of squeezing, antibunching results due to a reduction in the intensity fluctuations of the incoherent component. This differs from the case for small squeezing. For small squeezing antibunching results from an interference of the coherent component with the incoherent component.

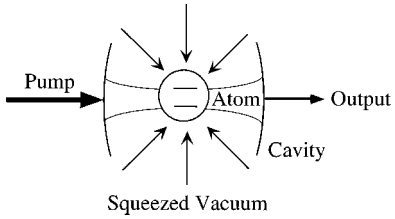

FIG. 1. Physical scheme.

In Sec. II we derive a generalized second-order Fokker-Planck equation. By eliminating the cavity mode adiabatically we obtain a Fokker-Plank equation in the bad-cavity limit. We then solve the associated Ito stochastic differential equations for the atomic variables in the steady state. In Sec. III we study the effects of a squeezed vacuum on atomic inversion. Section IV discusses photon statistics of the transmitted light. In Secs. V and VI we calculate the spectrum and the second-order intensity correlation function of the fluorescent light. Finally, in Sec. VII the main results of the paper are summarized.

II. FOKKER-PLANCK EQUATION

We consider a single two-level atom with transition frequency ω_a interacting with a damped cavity mode of resonance frequency ω_c. The atom is coupled to a broadband squeezed vacuum centered about the atomic resonance frequency ω_a and the cavity is driven by a classical field of amplitude ϵ and frequency ω_o. An outline of this system is shown in Fig. 1. The equation of motion for the density operator in a frame rotating at the frequency of the driving field ω_o is obtained as

$$\frac{\partial\hat{\rho}}{\partial t}=-i\Delta_c[\hat{a}^\dagger\hat{a},\hat{\rho}]-i\Delta_a[\hat{s}_z,\hat{\rho}]+g[\hat{a}^\dagger\hat{s}_--\hat{a}\hat{s}_+,\hat{\rho}]+\epsilon[\hat{a}^\dagger-\hat{a},\hat{\rho}]+\frac{\gamma}{2}(N+1)(2\hat{s}_-\hat{\rho}\hat{s}_+-\hat{s}_+\hat{s}_-\hat{\rho}-\hat{\rho}\hat{s}_+\hat{s}_-)$$
$$+\frac{\gamma}{2}N(2\hat{s}_+\hat{\rho}\hat{s}_--\hat{s}_-\hat{s}_+\hat{\rho}-\hat{\rho}\hat{s}_-\hat{s}_+)+\gamma(M\hat{s}_+\hat{\rho}\hat{s}_++M^*\hat{s}_-\hat{\rho}\hat{s}_-)+\kappa(2\hat{a}\hat{\rho}\hat{a}^\dagger-\hat{a}^\dagger\hat{a}\hat{\rho}-\hat{\rho}\hat{a}^\dagger\hat{a}), \quad (1)$$

where g is the atom-field coupling constant, $\hat{a}$ and $\hat{a}^\dagger$ are the annihilation and creation operators for the cavity mode, and $\hat{s}_+$, $\hat{s}_-$, and $\hat{s}_z$ are spin-half angular momentum operators describing the two-level atom and obeying the commutation relations $[\hat{s}_+,\hat{s}_-]=2\hat{s}_z$ and $[\hat{s}_\pm,\hat{s}_z]=\mp\hat{s}_\pm$. $\Delta_c=\omega_c-\omega_o$ and $\Delta_a=\omega_a-\omega_o$ are, respectively, the cavity and atomic detunings from the driving field, γ is the atomic decay rate for spontaneous emission into an ordinary vacuum, 2κ is the rate at which the cavity is losing photons, N is the mean photon number of the squeezed reservoir, and M is a parameter related to the phase correlations of the squeezed reservoir. They are related to the squeezing parameter r and its phase θ relative to the driving field by $N=\sinh^2(r)$ and $M=e^{i\theta}\sinh(r)\cosh(r)$. This choice of phase differs from that used in Refs. [11,12] by $\pi/2$. We express the density operator $\hat{\rho}(t)$ as [14,17]

$$\hat{\rho}(t)=\int P(\alpha,\alpha^*,\mu,\mu^*,m)|\alpha\rangle\langle\alpha|$$
$$\times[2m\hat{s}_z+1/2+\mu\hat{s}_++\mu^*\hat{s}_-]d^2\alpha d^2\mu dm, \quad (2)$$

where $|\alpha\rangle$ is a coherent state of $\hat{a}$ with eigenvalue α. Here α, α^*, μ, μ^*, and m are c-number variables corresponding to the operators $\hat{a}$, $\hat{a}^\dagger$, $\hat{s}_-$, $\hat{s}_+$, and $\hat{s}_z$, respectively. Substituting Eq. (2) into Eq. (1) and following the procedure used by Wang and Vyas [14], we obtain the following Fokker-Planck equation:

$$\frac{\partial}{\partial t}P(\alpha,\alpha^*,\mu,\mu^*,m)=\left\{-\frac{\partial}{\partial\alpha}[g\mu-(\kappa+i\Delta_c)\alpha+\epsilon]-\frac{\partial}{\partial\mu}\left[2gm\alpha-\left(\frac{\gamma}{2}(2N+1)+i\Delta_a\right)\mu+\gamma\mu^*M\right]\right.$$
$$\left.+\frac{\partial}{\partial m}\left[g\mu\alpha^*+\frac{\gamma}{2}\left((2N+1)m+\frac{1}{2}\right)\right]-\frac{\partial^2}{\partial\mu\partial\alpha}g\mu^2+\frac{\partial^2}{\partial\mu\partial\alpha^*}\left(\frac{1}{2}+m-\mu^*\mu\right)g-\frac{\partial^2}{\partial m\partial\alpha}g\left(\frac{1}{2}+m\right)\mu\right\}$$
$$\times P(\alpha,\alpha^*,\mu,\mu^*,m)+\text{c.c.} \quad (3)$$

This is an exact second-order Fokker-Planck equation obtained by using the mapping scheme defined by Eq. (2) without any system-size expansion or truncation of the resulting equation. The drift terms (terms inside the square brackets) depend on the degree of squeezing and the relative phase between the squeezed vacuum and the driving field via M. The diffusion terms (terms inside parentheses and coefficients of the second-order derivative terms) are identical to the diffusion terms in the Fokker-Planck equation of a single two-level atom decaying into ordinary vacuum and placed inside a coherently driven cavity [14].

In the bad-cavity limit ($2\kappa\gg\gamma$), the field variables decay much faster than the atomic variables. We can then eliminate the field variables adiabatically by setting partial derivatives with respect to α and α^* equal to zero in Eq. (3) leading to [14,17]

$$\alpha P=\frac{1}{\kappa+i\Delta_c}\left[\epsilon+g\mu+\frac{\partial}{\partial\mu}g\mu^2-\frac{\partial}{\partial\mu^*}\left(\frac{1}{2}+m-\mu^*\mu\right)g+\frac{\partial}{\partial m}g\left(\frac{1}{2}+m\right)\mu\right]. \tag{4}$$

On substituting Eq. (4) and its complex conjugate into Eq. (3) and simplifying the resulting expression we obtain Fokker-Planck equation in the bad-cavity limit as

$$\begin{aligned}\frac{1}{\gamma}\frac{\partial P}{\partial t}=\Bigg\{&-\frac{\partial}{\partial\mu}\left[-\frac{1}{2}[2C+2N+1-\delta_a\delta_c+i\delta_a+i\delta_c(2N+1)]\mu+M(1+i\delta_c)\mu^*+\frac{1}{\sqrt{2}}Ym\right](1+i\delta_c)^{-1}\\&+\frac{\partial}{\partial m}\left[\frac{1}{2\sqrt{2}}Y(1+i\delta_c)\mu+\frac{1}{4}(2C+1+\delta_c^2)(2m+1)+N(1+\delta_c^2)m\right](1+\delta_c^2)^{-1}\\&+\frac{\partial^2}{\partial m^2}\left[\frac{C}{2}(2m+1)\mu\mu^*\right](1+\delta_c^2)^{-1}+\frac{\partial^2}{\partial\mu\partial\mu^*}[Cm(1+2m-2\mu\mu^*)](1+\delta_c^2)^{-1}\\&-\frac{\partial^2}{\partial\mu^2}[2Cm\mu^2](1+i\delta_c)^{-1}-\frac{\partial^2}{\partial m\partial\mu}\left[\frac{C\mu}{2}[(2m+1)^2-4\mu\mu^*-i\delta_c(4m^2-1)]\right](1+\delta_c^2)^{-1}\Bigg\}P+\text{c.c.},\end{aligned} \tag{5}$$

where we have introduced the dimensionless parameters

$$C=\frac{g^2}{\gamma\kappa},\quad Y=\frac{2\sqrt{2}g\epsilon}{\kappa\gamma},\quad \delta_a=\frac{\Delta_a}{\gamma/2}=\frac{\omega_a-\omega_0}{\gamma/2},$$

$$\delta_c=\frac{\Delta_c}{\kappa}=\frac{\omega_c-\omega_0}{\kappa}. \tag{6}$$

Note that the diffusion terms are still independent of the squeezed vacuum. As a check we note that for $N=M=0$ it reduces to the Fokker-Planck equation for a single two-level atom coupled to the ordinary vacuum [14].

Taking the average value of the atomic variables we arrive at the optical Bloch equations

$$\frac{\partial}{\partial t}\langle\mu\rangle=-\left(\frac{\gamma_{eff}}{2}+i\Delta_{eff}\right)\langle\mu\rangle+M\gamma\langle\mu^*\rangle-i\Omega_{eff}\langle m\rangle, \tag{7}$$

$$\frac{\partial}{\partial t}\langle\mu^*\rangle=-\left(\frac{\gamma_{eff}}{2}-i\Delta_{eff}\right)\langle\mu^*\rangle+M^*\gamma\langle\mu\rangle+i\Omega_{eff}^*\langle m\rangle, \tag{8}$$

$$\frac{\partial}{\partial t}\langle m\rangle=-\gamma_{eff}\left(\langle m\rangle+\frac{1}{2}\right)+\gamma N+\frac{i}{2}(\Omega_{eff}\langle\mu^*\rangle-\Omega_{eff}^*\langle\mu\rangle), \tag{9}$$

where

$$\gamma_{eff}=\gamma\left(2N+1+\frac{2C}{1+\delta_c^2}\right),\Delta_{eff}=\frac{\gamma}{2}\left(\delta_a-\frac{2\delta_cC}{1+\delta_c^2}\right),$$

$$\Omega_{eff}=\frac{i\gamma Y}{\sqrt{2}(1+i\delta_c)}. \tag{10}$$

Once again, for the ordinary vacuum ($N=|M|=0$), Eqs. (7)–(9) reduce to those obtained by Wang and Vyas [15]. It can be seen that the coupling of the atom to a squeezed vacuum enhances the atomic decay rate from $\gamma[1+2C/(1+\delta_c^2)]$ to $\gamma[2N+1+2C/(1+\delta_c^2)]$, introduces phase sensitive terms in Eq. (7) and (8), and adds a constant term proportional to the mean photon number of the squeezed vacuum in Eq. (9). It should be pointed out that, except for the phase dependent terms, such terms would also arise when we consider the coupling of an atom to a finite temperature thermal reservoir. The results for the atom coupled to a thermal reservoir can be obtained by substituting $M=0$.

We introduce the polarization quadratures defined by

$$\langle\mu\rangle=\langle\mu_x\rangle-i\langle\mu_y\rangle,\quad \langle\mu^*\rangle=\langle\mu_x\rangle+i\langle\mu_y\rangle. \tag{11}$$

Then we can write the optical Bloch equation in the form

$$\frac{\partial}{\partial t}\langle\mu_x\rangle=-\gamma_x\langle\mu_x\rangle-[|M|\gamma\sin(\theta)+\Delta_{eff}]\langle\mu_y\rangle+\frac{\gamma Y}{\sqrt{2}(1+\delta_c^2)}\langle m\rangle, \tag{12}$$

$$\frac{\partial}{\partial t}\langle\mu_y\rangle=-\gamma_y\langle\mu_y\rangle-[|M|\gamma\sin(\theta)-\Delta_{eff}]\langle\mu_y\rangle+\frac{\gamma Y\delta_c}{\sqrt{2}(1+\delta_c^2)}\langle m\rangle, \tag{13}$$

$$\frac{\partial}{\partial t}\langle m\rangle=-(\gamma_x+\gamma_y)\langle m\rangle-\frac{\gamma Y}{\sqrt{2}(1+\delta_c^2)}[\langle\mu_x\rangle+\delta_c\langle\mu_y\rangle]-\frac{\gamma}{2}\left(1+\frac{2C}{1+\delta_c^2}\right), \tag{14}$$

where

$$\gamma_x=\frac{\gamma}{2}\left(1+2N-2|M|\cos(\theta)+\frac{2C}{1+\delta_c^2}\right), \tag{15}$$

$$\gamma_y=\frac{\gamma}{2}\left(1+2N+2|M|\cos(\theta)+\frac{2C}{1+\delta_c^2}\right). \tag{16}$$

Comparison of Eqs. (12)–(14) with those obtained for resonance fluorescence with an injected squeezed vacuum by Rice and Pedrotti [11] we find the following differences. Equations (12)–(14) include the effects of atomic and cavity detunings on the decay rates of the polarization quadratures. The presence of the factor $(1+\delta_c^2)^{-1}$ in the decay rates γ_x and γ_y reduces the enhancement of spontaneous emission due to cavity when the cavity mode is detuned with respect to the driving field. Another difference is that the enhancement of spontaneous emission due to a squeezed vacuum is not affected by the atomic cooperativity parameter C. This, of course, is a consequence of the direct coupling of the atom to the squeezed vacuum rather than through the lossy cavity mirror, which is the case in resonance fluorescence with injected squeezed vacuum. Thus for weak atom-cavity coupling ($C<1$) the spontaneous emission rate is enhanced much more when the squeezed vacuum is directly coupled to the atom than when it is coupled through the mirror.

III. ATOMIC INVERSION

To study the effects of detuning and squeezed vacuum on atomic inversion we solve the optical Bloch equations in the steady state $\langle\dot{\mu}_x\rangle=\langle\dot{\mu}_y\rangle=\langle\dot{m}\rangle=0$. Using this in Eqs. (12)–(14) and solving for the averages we get

$$\langle\mu_x\rangle_{ss}=-\frac{\gamma Y(\gamma_{eff}-2\gamma N)}{\sqrt{2}\mathcal{R}}\{(\gamma_{eff}-2\delta_c\Delta_{eff}) +2\gamma|M|[\cos(\theta)-\delta_c\sin(\theta)]\}, \tag{17}$$

$$\langle\mu_y\rangle_{ss}=-\frac{\gamma Y(\gamma_{eff}-2\gamma N)}{\sqrt{2}\mathcal{R}}\{(\gamma_{eff}\delta_c+2\Delta_{eff}) -2\gamma|M|[\sin(\theta)+\delta_c\cos(\theta)]\}, \tag{18}$$

$$\langle m\rangle_{ss}=-\frac{2(1+\delta_c^2)(\gamma_{eff}-2\gamma N)}{\mathcal{R}} \times\left(\frac{\gamma_{eff}^2}{4}+\Delta_{eff}^2-|M|^2\gamma^2\right). \tag{19}$$

Here the denominator $\mathcal{R}$ is given by

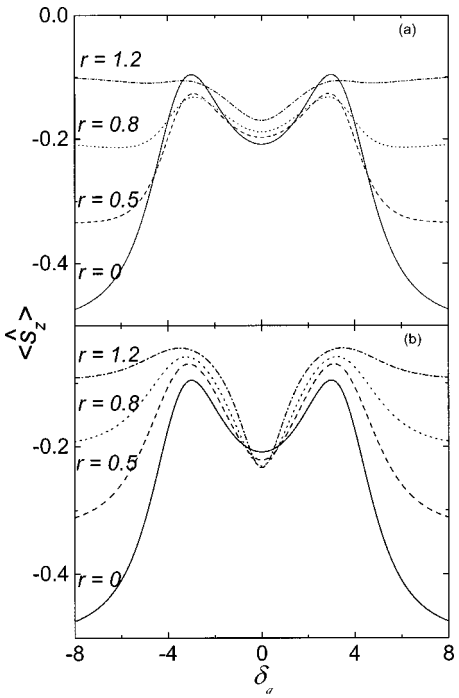

FIG. 2. The atomic inversion $\langle\hat{s}_z\rangle$ as a function of atomic detuning parameter δ_a in the weak-field and weak-coupling limit for different values of squeezing parameter r, pump parameter $Y=3$, $C=0.4$, $\delta_c=\delta_a$, and (a) $\theta=0$, (b) $\theta=\pi$.

$$\mathcal{R}=4(1+\delta_c^2)\left(\frac{\gamma_{eff}^2}{4}+\Delta_{eff}^2-|M|^2\gamma^2\right)\gamma_{eff} +\gamma^2Y^2\left[\gamma_{eff}+2|M|\gamma\left(\frac{1-\delta_c^2}{1+\delta_c^2}\right)\cos(\theta) -4\gamma|M|\left(\frac{\delta_c}{1+\delta_c^2}\right)\sin(\theta)\right]. \tag{20}$$

Atomic inversion in the steady state is given by Eq. (19). For the special case where the atomic and cavity detuning parameters are equal ($\delta_c=\delta_a$), the dependence of atomic inversion on detuning is shown in Fig. 2. Figure 2(a) shows inversion when the squeezed vacuum is in phase ($\theta=0$) with the coherent excitation. For the ordinary vacuum ($r=0$) we see that the inversion has a single peak at zero atomic detuning and for large detunings it approaches -0.5, indicating that the atom is most likely to be in the ground state [14]. For nonzero squeezing the overall effect of increasing the squeezing parameter r is to increase atomic inversion far away from the resonance. This is because, even when the driving field is detuned from the atom, the atom still senses the broadband squeezed vacuum. Consequently, as r increases the number of quanta in the squeezed vacuum increases, resulting in an increase in atomic inversion. In general, for $\theta=0$ atomic inversion increases monotonically with increase in the squeezing parameter r for all values of detunings, and as a function of detuning it shows a single peak for all values of r.

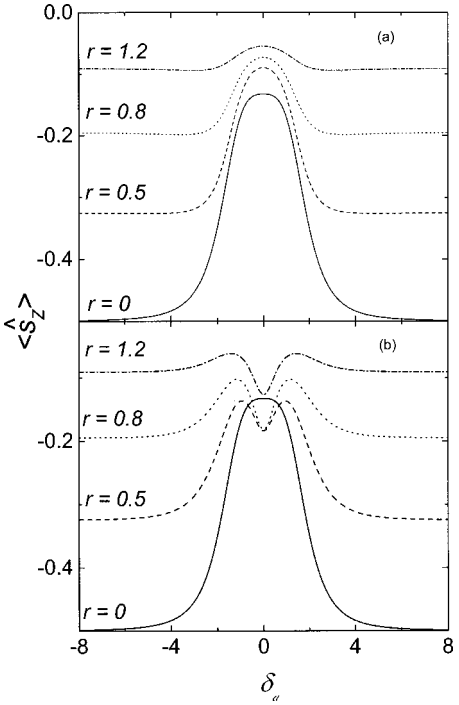

FIG. 3. The atomic inversion $\langle \hat{s}_z \rangle$ as a function of atomic detuning parameter δ_a in the strong-field and strong-coupling limit for different values of squeezing parameter r, pump parameter $Y=13$, $C=5$, $\delta_c=\delta_a$, and (a) $\theta=0$, (b) $\theta=\pi$.

Figure 2(b) shows inversion when the squeezed vacuum is out of phase with the driving field ($\theta=\pi$). Far away from the resonance, the behavior of the inversion is similar to that for $\theta=0$ [Fig. 2(a)]. However, near resonance atomic inversion shows interesting features. On-resonance atomic inversion can fall below its value for the ordinary vacuum ($r=0$). The on-resonance inversion initially decreases as r increases. With further increase in r, it rises above its value for the ordinary vacuum. Another interesting feature is that for small values of r the atomic inversion shows two peaks located symmetrically at nonzero atomic detuning. This behavior near resonance is similar to vacuum Rabi splitting. The presence of squeezed light effectively reduces the threshold value of C for seeing the vacuum Rabi splitting. With increase in r the two peaks broaden and eventually disappear leaving a dip for large values of r. Thus the peaks seen in the atomic inversion are phase sensitive as they are not seen when the squeezed vacuum is in phase ($\theta=0$) with the coherent excitation. These peaks are also absent when the atom decays into a nonzero temperature thermal reservoir.

Figure 3 shows inversion as a function of atomic detuning in the strong-field and strong-coupling limits. In this regime for $r=0$ the inversion shows two symmetric peaks as a function of detuning due to vacuum Rabi splitting, which is in agreement with the results for an atom decaying to the ordinary vacuum [14]. As the squeezing parameter r increases the two peaks broaden and for large values of r the peaks disappear. In Fig. 3(a), which is for the phase $\theta=0$, the on-resonance inversion monotonically increases with increase in the squeezing parameter r. On the other hand, the amplitudes of the two peaks first decrease as r increases before increasing with further increase in r, ultimately rising above the value for the ordinary vacuum. For very large values of r the peaks disappear. In Fig. 3(b), which is for $\theta=\pi$, inversion behaves differently. The on-resonance inversion first decreases with increase in r, but then increases as r increases further and rises above its value for the ordinary vacuum. The amplitudes of the two symmetric peaks increase monotonically as the squeezing parameter r increases. Thus when an atom decays to the squeezed vacuum the inversion is phase sensitive. This is to be compared with an atom decaying into a nonzero temperature thermal reservoir. In that case the inversion increases monotonically with increase in thermal photons and does not display any phase sensitive features.

IV. PHOTON STATISTICS OF THE TRANSMITTED LIGHT

The photon statistics of the transmitted light at the output mirrors are related to the statistics of the cavity mode. The expectation values of the field variables are calculated by first expressing them in normal order and then replacing them by corresponding c numbers. The c numbers corresponding to field variables are then expressed in terms of atomic variables. Then field averages are calculated in terms of atomic averages. Using the adiabatic formula given in Eq. (4) we can show that the moments of field operators can be expressed as [14]

$$\langle (\hat{a}^\dagger)^p \hat{a}^q \rangle = \langle (\alpha^*)^p \alpha^q \rangle = \frac{n_s{}^{(p+q)/2} Y^{p+q-2}}{(1-i\delta_c)^p (1+i\delta_c)^q} \times [2\sqrt{2} CY(p\langle \mu^* \rangle + q\langle \mu \rangle) + 4C^2 pq(1+2\langle m \rangle) + Y^2], \tag{21}$$

where $n_s=\gamma^2/8g^2$ is the saturation photon number and Y and C are defined in Eq. (6). Using Eq. (21) we obtain the steady state intracavity field amplitude as

$$X = \frac{\langle \alpha \rangle}{\sqrt{n_s}} = \frac{Y}{1+i\delta_c}[2\sqrt{2} C\langle \mu \rangle_{ss} + Y], \tag{22}$$

and the steady-state two-time intensity correlation function as

$$g^{(2)}(0) = \frac{Y^2[Y^2 + 8\sqrt{2} CY\langle \mu_x \rangle_{ss} + 16C^2(1+2\langle m \rangle_{ss})]}{[Y^2 + 4\sqrt{2} CY\langle \mu_x \rangle_{ss} + 4C^2(1+2\langle m \rangle_{ss})]^2}, \tag{23}$$

where $\langle \mu_x \rangle_{ss}$ and $\langle m \rangle_{ss}$ are given by Eqs. (17) and (19).

Figure 4 shows on-resonance $g^{(2)}(0)$ for the transmitted light as a function of squeezing parameter r for $\theta=0$ and π in the weak-coupling and weak-driving-field limits. For $r=0$, $g^{(2)}(0)$ is nearly zero, reflecting maximum antibunching. As r increases, $g^{(2)}(0)$ increases and becomes larger than unity, reflecting bunching. As r is increased further

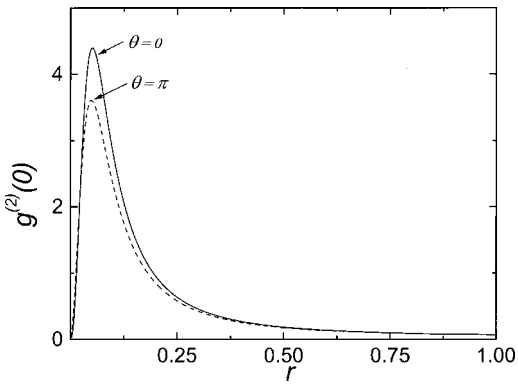

FIG. 4. Second-order intensity correlation function $g^{(2)}(0)$ of the transmitted light as a function of squeezing parameter r for $\theta=0$ and π. Other parameters for the curves are $Y=0.1$, $C=0.5$, and $\delta_c=\delta_a=0$. $g^{(2)}(0)<1$ reflects the nonclassical effect of antibunching.

$g^{(2)}(0)$ reaches a maximum before decreasing to very small values. Thus for very large values of r the transmitted light again shows antibunching.

Figure 5 shows $g^{(2)}(0)$ as a function of detuning for several different values of r in the weak-coupling and weak-driving-field limits when $\theta=0$. Figure 5(a) is plotted for $\delta_c=0$. In this case $g^{(2)}(0)$ shows a dip as a function of detuning for $r=0$, so that maximum antibunching is seen on resonance in agreement with Ref. [14]. As r increases we find that the on-resonance value of $g^{(2)}(0)$ increases, indicating

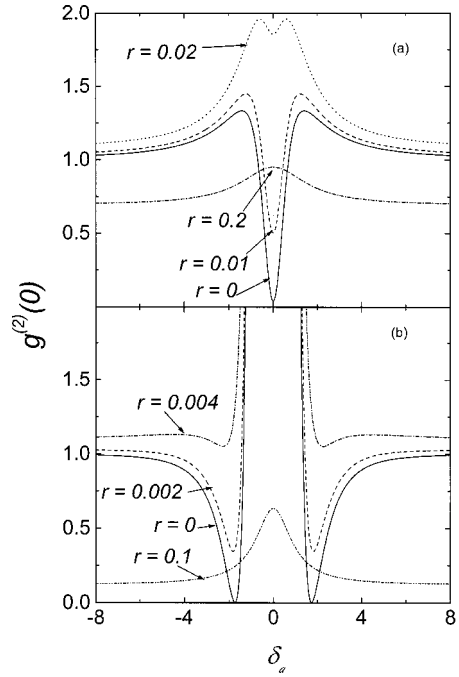

FIG. 5. Second-order intensity correlation function $g^{(2)}(0)$ of the transmitted light as a function of atomic detuning parameter δ_a for pumping parameter $Y=0.1$, $\theta=0$, and different values of r. Other parameters for the curves are (a) $C=0.5$ and $\delta_c=0$; (b) $C=2$ and $\delta_c=-\delta_a$. $g^{(2)}(0)<1$ reflects the nonclassical effect of antibunching.

increased bunching of transmitted light. For small squeezing $g^{(2)}(0)$ shows a two-peak structure as a function of detuning. As r is increased further we find that $g^{(2)}(0)$ exhibits a single peak. It is interesting to note that for sufficiently large squeezing $g^{(2)}(0)$ for all values of detuning decreases to be less than unity, reflecting antibunching of the transmitted light.

Figure 5(b) shows $g^{(2)}(0)$ for $\delta_c=-\delta_a$ and a larger value of C than that in Fig. 5(a). For $r=0$ we find that $g^{(2)}(0)$ shows two dips at nonzero detuning and a peak at zero detuning. Thus antibunching is seen at nonzero detuning, whereas at zero detuning we see bunching. For very small increase in r, $g^{(2)}(0)$ increases and antibunching disappears altogether. As r increases further, $g^{(2)}(0)$ becomes less than unity and shows a single peak as a function of detuning. Thus for very large values of r the transmitted light shows antibunching for all values of detuning.

The behavior of $g^{(2)}(0)$ can be explained in terms of self-homodyning of coherent and incoherent components of the intracavity field. The intracavity field can be divided into two parts, coherent and incoherent components, as

$$\hat{a}=\langle\hat{a}\rangle+\Delta\hat{a}. \tag{24}$$

Equation (22) indicates that for nonzero detuning and arbitrary values of θ the intracavity field is not in phase with the driving field. The relative phase ϕ between the coherent component and the driving field is given by

$$\tan(\phi)=\frac{2\sqrt{2}C\langle\mu_y\rangle_{ss}+\delta_c(Y+2\sqrt{2}C\langle\mu_x\rangle_{ss})}{\delta_c 2\sqrt{2}C\langle\mu_y\rangle_{ss}-(Y+2\sqrt{2}C\langle\mu_x\rangle_{ss})}. \tag{25}$$

We introduce a field quadrature which is in phase with the driving field as

$$\hat{A}_1=\frac{1}{2}(\hat{a}e^{-i\phi}+\hat{a}^{\dagger}e^{i\phi}). \tag{26}$$

Using Eqs. (26) and (21), fluctuations in $\hat{A}_1$ are calculated to be

$$\langle:(\Delta\hat{A}_1)^2:\rangle=\frac{2C^2n_s}{(1+\delta_c^2)}[(1+\langle m\rangle_{ss})-4(\langle\mu_x\rangle_{ss}^2+\langle\mu_y\rangle_{ss}^2)]. \tag{27}$$

In terms of the coherent and incoherent components we can rewrite $g^{(2)}(0)$ as

$$g^{(2)}(0)=1+G_1+G_2+G_3, \tag{28}$$

where

$$G_1=\frac{4|\langle\hat{a}\rangle|^2\langle:\Delta\hat{A}_1^2:\rangle}{(|\langle\hat{a}\rangle|^2+\langle\Delta\hat{a}^{\dagger}\Delta\hat{a}\rangle)^2}, \tag{29}$$

$$G_2=\frac{2(\langle\hat{a}\rangle\langle\Delta\hat{a}^{\dagger 2}\Delta\hat{a}\rangle+\text{c.c.})}{(|\langle\hat{a}\rangle|^2+\langle\Delta\hat{a}^{\dagger}\Delta\hat{a}\rangle)^2}, \tag{30}$$

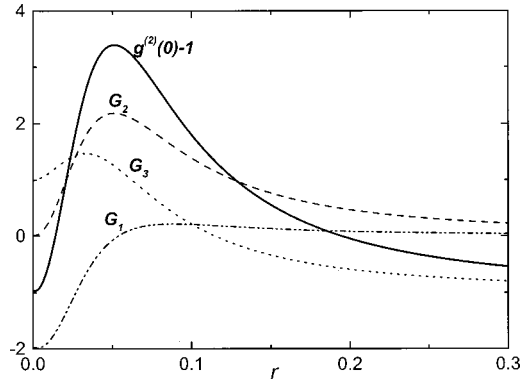

FIG. 6. G_1, G_2, G_3, and $g^{(2)}(0)-1$ of the transmitted light as functions of squeezing parameter r for $\theta=0$. Other parameters for the curves are $Y=0.1$, $C=0.5$, and $\delta_c=\delta_a=0$. $g^{(2)}(0)-1<0$ reflects the nonclassical effect of antibunching.

$$G_3=\frac{\langle\Delta\hat{a}^{\dagger 2}\Delta\hat{a}^2\rangle-\langle\Delta\hat{a}^{\dagger}\Delta\hat{a}\rangle^2}{(|\langle\hat{a}\rangle|^2+\langle\Delta\hat{a}^{\dagger}\Delta\hat{a}\rangle)^2}. \tag{31}$$

In Fig. 6 we show on-resonance behavior of G_1, G_2, G_3, and $[g^{(2)}(0)-1]$ for $\theta=0$ as a function of squeezing parameter. The other parameters are the same as those for Fig. 4. Here G_1 describes the interference of the coherent component with the fluctuations in the quadrature $\hat{A}_1$. G_1 is less than zero when the quadrature $\hat{A}_1$ is squeezed. This term is responsible for antibunching for very small values of r. As r increases, squeezing in quadrature $\hat{A}_1$ decreases and therefore G_1 increases. For large values of r, G_1 is positive. The contribution of G_2 is always positive and therefore reduces antibunching. G_3 is the contribution of intensity fluctuations in the incoherent component of the field. It becomes negative for large values of r, again leading to antibunching. Thus antibunching of the transmitted light for small values of r is due to squeezing in quadrature $\hat{A}_1$, whereas for large values of r it is due to reduction in intensity fluctuations of the incoherent component.

V. SPECTRUM OF THE FLUORESCENT LIGHT

Next we calculate the spectrum of the fluorescent light. The spectrum of the fluorescent light is defined as

$$S(\omega)=\frac{1}{2\pi}\int_{-\infty}^{\infty}d\tau\exp[i(\omega-\omega_a)\tau]\langle\hat{s}_+(0)\hat{s}_-(\tau)\rangle_{ss}$$
$$=\frac{1}{\pi}\mathrm{Re}\left[\int_0^{\infty}d\tau\exp[i(\omega-\omega_a)\tau]\langle\hat{s}_+(0)\hat{s}_-(\tau)\rangle_{ss}\right]. \tag{32}$$

Using the polarization quadratures defined in Eqs. (11), the two-time correlation function $\langle\hat{s}_+(0)\hat{s}_-(\tau)\rangle_{ss}$ can be written as

$$\langle\hat{s}_+(0)\hat{s}_-(\tau)\rangle_{ss}=\langle\hat{s}_x(0)\hat{s}_x(\tau)\rangle_{ss}+\langle\hat{s}_y(0)\hat{s}_y(\tau)\rangle_{ss}$$
$$-i(\langle\hat{s}_y(0)\hat{s}_x(\tau)\rangle_{ss}-\langle\hat{s}_x(0)\hat{s}_y(\tau)\rangle_{ss}). \tag{33}$$

The general analytic expressions for the correlations needed for the spectrum are cumbersome in the presence of detuning and for arbitrary values of θ. Here we present calculations of the spectrum only for the resonant case ($\delta_a=\delta_c=0$) and for $\theta=0$ or π. We obtain the correlation needed for calculating the spectrum by using the quantum regression theorem with initial conditions

$$\langle\hat{s}_x(0)^2\rangle_{ss}=\langle\hat{s}_y(0)^2\rangle_{ss}=1/4,$$
$$\langle\hat{s}_x(0)\hat{s}_y(0)\rangle_{ss}=-\langle\hat{s}_y(0)\hat{s}_x(0)\rangle_{ss}=(i/2)\langle m\rangle_{ss},$$
$$\langle\hat{s}_x(0)\hat{s}_z(0)\rangle_{ss}=-\langle\mu_y\rangle_{ss},$$
$$\langle\hat{s}_y(0)\hat{s}_z(0)\rangle_{ss}=-\langle\mu_x\rangle_{ss}. \tag{34}$$

We first present results for the spectrum of the fluorescent light in the weak-driving-field limit $Y\leqslant Y_{th}$, where the threshold driving field Y_{th} is given by

$$Y_{th}=\frac{\gamma_0-\gamma_{\mp}}{\sqrt{2}\gamma}, \tag{35}$$

with

$$\gamma_-=\frac{\gamma}{2}(1+2C+2N-2|M|),$$
$$\gamma_+=\frac{\gamma}{2}(1+2C+2N+2|M|), \tag{36}$$
$$\gamma_0=\gamma(1+2C+2N).$$

Here γ_- corresponds to the threshold driving field for phase $\theta=0$ and γ_+ corresponds to the threshold driving field for $\theta=\pi$. We will follow the convention that the upper sign corresponds to phase $\theta=0$ and the lower sign corresponds to phase $\theta=\pi$. Below threshold all the eigenvalues λ_1, λ_2, and λ_3 given by Eq. (42) or (43) are real and we obtain the following expression for the two-time correlation function:

$$\langle\hat{s}_+(0)\hat{s}_-(\tau)\rangle_{ss}=C_0+C_1\exp(\lambda_1\tau)+C_2\exp(\lambda_2\tau)$$
$$+C_3\exp(\lambda_3\tau), \tag{37}$$

where

$$C_0=\langle\mu_x\rangle_{ss}^2, \tag{38}$$

$$C_1=(1+2\langle m\rangle_{ss})/4, \tag{39}$$

$$C_2=\frac{\lambda_2+\gamma_0}{\lambda_2-\lambda_3}\left[C_1\left(1-\frac{2\sqrt{2}(\gamma_0+\lambda_3)}{\gamma Y}\langle\mu_x(0)\rangle_{ss}\right)-C_0\right], \tag{40}$$

$$C_3=\frac{\lambda_3+\gamma_0}{\lambda_3-\lambda_2}\left[C_1\left(1-\frac{2\sqrt{2}(\gamma_0+\lambda_2)}{\gamma Y}\langle\mu_x(0)\rangle_{ss}\right)-C_0\right]. \tag{41}$$

The eigenvalues λ_1, λ_2, and λ_3 for $\theta=0$ are

$$\lambda_1=-\gamma_+,$$

$$\lambda_2=\frac{1}{2}[-(\gamma_0+\gamma_-)+\sqrt{(\gamma_0-\gamma_-)^2-2(Y\gamma)^2}], \tag{42}$$

$$\lambda_3=\frac{1}{2}[-(\gamma_0+\gamma_-)-\sqrt{(\gamma_0-\gamma_-)^2-2(Y\gamma)^2}],$$

and for $\theta=\pi$ they are

$$\lambda_1=-\gamma_-,$$

$$\lambda_2=\frac{1}{2}[-(\gamma_0+\gamma_+)+\sqrt{(\gamma_0-\gamma_+)^2-2(Y\gamma)^2}], \tag{43}$$

$$\lambda_3=\frac{1}{2}[-(\gamma_0+\gamma_+)-\sqrt{(\gamma_0-\gamma_+)^2-2(Y\gamma)^2}].$$

The expectation values $\langle\mu_x\rangle_{ss}$ and $\langle m\rangle_{ss}$ are found from Eqs. (17) and (18) to be

$$\langle\mu_x\rangle_{ss}=-\frac{\gamma^2Y(1+2C)}{\sqrt{2}[(\gamma Y)^2+2\gamma_0\gamma_\mp]},$$

$$\langle m\rangle_{ss}=-\frac{\gamma\gamma_\mp(1+2C)}{(\gamma Y)^2+2\gamma_0\gamma_\mp}. \tag{44}$$

Employing Eq. (37) in the expression for the spectrum, we obtain

$$S(\omega)=\left[C_0\delta(\omega-\omega_a)-\frac{C_1}{\pi}\frac{\lambda_1}{\lambda_1^2+(\omega-\omega_a)^2}-\frac{C_2}{\pi}\frac{\lambda_2}{\lambda_2^2+(\omega-\omega_a)^2}-\frac{C_3}{\pi}\frac{\lambda_3}{\lambda_3^2+(\omega-\omega_a)^2}\right]. \tag{45}$$

Equation (45) indicates that in the weak-driving limit the spectrum is composed of a coherent component given by the δ function term and an incoherent component given by the sum of three Lorenzians centered at the atomic resonance frequency ω_a of widths $2\lambda_1$, $2\lambda_2$, and $2\lambda_3$, respectively. In Fig. 7 the incoherent part of the spectrum is shown for different values of the squeezing parameter r. In general the effect of the squeezed vacuum is to narrow the width of the spectrum. In the weak-driving limit the spectrum is not very sensitive to phase. We have, therefore, shown the curves for only $\theta=\pi$.

In the strong-driving-field limit $Y>Y_{th}$, λ_2 and λ_3 given by Eq. (42) or (43) become complex and the spectrum takes the form

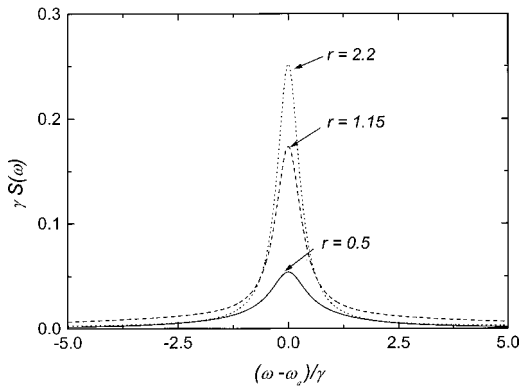

FIG. 7. Spectrum of the fluorescent light below threshold for different values of r, $Y=0.11$, $C=0.3$, and $\theta=\pi$.

$$S(\omega)=\left[C_0\delta(\omega-\omega_a)-\frac{C_1}{\pi}\frac{\lambda_1}{\lambda_1^2+(\omega-\omega_a)^2}-\frac{1}{\pi}\frac{C_R\lambda_R+C_I(\omega-\omega_a+\lambda_I)}{\lambda_R^2+(\omega-\omega_a+\lambda_I)^2}-\frac{1}{\pi}\frac{C_R\lambda_R-C_I(\omega-\omega_a-\lambda_I)}{\lambda_R^2+(\omega-\omega_a-\lambda_I)^2}\right] \tag{46}$$

where

$$\lambda_R=-\frac{1}{2}(\gamma_0+\gamma_\mp),\quad \lambda_I=\frac{1}{2}\sqrt{2(\gamma Y)^2-(\gamma_0-\gamma_\mp)^2}, \tag{47}$$

$$C_R=\frac{1}{2}[C_1-C_0], \tag{48}$$

$$C_I=-\frac{\gamma_0+\lambda_R}{2\lambda_I}\left[(C_1-C_0)-C_1\langle\mu_x\rangle_{ss}\frac{2\sqrt{2}(\gamma_0+\lambda_R)}{\gamma Y}\times\left\{1+\left(\frac{\lambda_I}{\gamma_0+\lambda_R}\right)^2\right\}\right]. \tag{49}$$

The incoherent part of the spectrum is shown in Fig. 8(a) for $\theta=0$ and in Fig. 8(b) for $\theta=\pi$ for several different values of the squeezing parameter r. The incoherent part of the spectrum has three peaks, similar to the Mollow spectrum. The central peak has full width at half maxima $2|\lambda_1|=2\gamma_\pm=\gamma(1+2C+2N\pm2|M|)$. The other two symmetrical peaks displaced by $\pm\lambda_I$ from the central peak have a width of $2|\lambda_R|=(\gamma_0+\gamma_\mp)=(\gamma/2)[3(1+2C+2N)\mp2|M|]$. When the driving field and the squeezed vacuum are out of phase ($\theta=\pi$), the width of the central peak γ_- decreases as the degree of squeezing r increases. For strong squeezing $r\gg1$, $N\simeq(e^{2r}-2)/4$ and $|M|\simeq e^{2r}/4$ so that the width of the central peak approaches a value $|\lambda_1|=\gamma C$ and the width of the sidebands approaches $\gamma(3C+e^{2r}/2)$ for $\theta=\pi$. Thus in this regime the central peak becomes narrower, whereas the sidebands become broader and eventually disappear for a very large value of r. When the driving field is in phase with

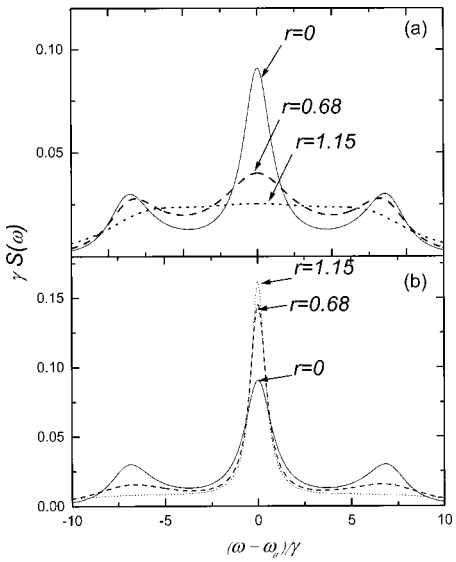

FIG. 8. Spectrum of the fluorescent light above threshold for different values of r and for $C=0.4$, $Y=10$; solid line $r=0$, dashed line $r=0.68$ and dotted line $r=1.15$. (a) $\theta=0$, (b) $\theta=\pi$.

the squeezed vacuum ($\theta=0$), the width of the central peak γ_+ increases as the degree of squeezing increases. For strong squeezing $r\gg1$, the width of the central peak approaches $\gamma(C+e^{2r}/2)$ and the width of the sidebands approaches $\gamma(3C+e^{2r})$ for $\theta=0$. Thus for a very large value of r all three peaks disappear. In the presence of a thermal reservoir the width of the central peak is $(\gamma/2)(1+2C+2N)$ and that of the sidebands is $(\gamma/2)[3(1+2C+2N)]$. The spectrum in the presence of a thermal reservoir does not show phase sensitivity and for a large number of thermal photons all three peaks disappear. It is interesting to note that the change in the width and the location of the peaks due to the squeezed reservoir is independent of the cooperativity parameter, whereas for the model considered by Rice and Pedrotti [11] the change in the width and location of the peaks due to squeezing depends on the cooperativity parameter. This is because the squeezed vacuum is injected into the cavity through the output mirror.

VI. SECOND-ORDER INTENSITY CORRELATION FUNCTION OF THE FLUORESCENT LIGHT

For completeness, in this section we study the second-order intensity correlation function of the fluorescent light in both the weak- and strong-driving-field limits. The second-order intensity correlation function

$$g^{(2)}(\tau)=\frac{\langle\hat{s}_+(0)\hat{s}_+(\tau)\hat{s}_-(\tau)\hat{s}_-(0)\rangle_{ss}}{\langle\hat{s}_+(0)\hat{s}_-(0)\rangle_{ss}^2} \tag{50}$$

is the probability of detecting a photon at a time τ given that one was detected at time 0. Using the relation $\hat{s}_+(\tau)\hat{s}_-(\tau)=\frac{1}{2}(2\hat{s}_z+1)$ we obtain

$$\langle\hat{s}_+(0)\hat{s}_+(\tau)\hat{s}_-(\tau)\hat{s}_-(0)\rangle_{ss}=\frac{1}{4}[4\langle\hat{s}_+(0)\hat{s}_z(\tau)\hat{s}_-(0)\rangle_{ss}+2\langle\hat{s}_z(0)\rangle_{ss}+1]. \tag{51}$$

By expressing $\hat{s}_+$ and $\hat{s}_-$ in terms of the polarization quadrature operators one can write

$$\begin{aligned}\langle\hat{s}_+(0)\hat{s}_z(\tau)\hat{s}_-(0)\rangle_{ss}=&[\langle\hat{s}_x(0)\hat{s}_z(\tau)\hat{s}_x(0)\rangle_{ss}\\&+\langle\hat{s}_y(0)\hat{s}_z(\tau)\hat{s}_y(0)\rangle_{ss}\\&-i(\langle\hat{s}_x(0)\hat{s}_z(\tau)\hat{s}_y(0)\rangle_{ss}\\&-\langle\hat{s}_y(0)\hat{s}_z(\tau)\hat{s}_x(0)\rangle_{ss})].\end{aligned} \tag{52}$$

The correlations in the above expression can be obtained by using the quantum regression theorem with the initial conditions

$$\langle\hat{s}_x(0)\hat{s}_z(0)\hat{s}_x(0)\rangle_{ss}=\langle\hat{s}_y(0)\hat{s}_z(0)\hat{s}_y(0)\rangle_{ss}-\langle m\rangle_{ss}/4, \tag{53}$$

$$\langle\hat{s}_y(0)\hat{s}_z(0)\hat{s}_x(0)\rangle_{ss}=-\langle\hat{s}_x(0)\hat{s}_z(0)\hat{s}_y(0)\rangle_{ss}=i/8, \tag{54}$$

$$\langle\hat{s}_x(0)\hat{s}_x(0)\hat{s}_x(0)\rangle_{ss}=-\langle\hat{s}_y(0)\hat{s}_x(0)\hat{s}_y(0)\rangle_{ss}=\langle\mu_x\rangle_{ss}/4, \tag{55}$$

$$\langle\hat{s}_x(0)\hat{s}_x(0)\hat{s}_y(0)\rangle_{ss}=\langle\hat{s}_y(0)\hat{s}_x(0)\hat{s}_x(0)\rangle_{ss}=\langle\mu_y\rangle_{ss}/4. \tag{56}$$

Using these correlations we find the second-order intensity correlation function for the fluorescent light defined in Eq. (50) to be

$$\begin{aligned}g^{(2)}(\tau)=1+&\frac{1}{(\lambda_2-\lambda_3)}\\&\times\left[\left\{(\gamma_0+\lambda_3)+\frac{\sqrt{2}\,\gamma Y\langle\mu_x\rangle_{ss}}{(1+2\langle m\rangle_{ss})}\right\}\right.\\&\times\exp(\lambda_2\tau)-\left\{(\gamma_0+\lambda_2)+\frac{\sqrt{2}\,\gamma Y\langle\mu_x\rangle_{ss}}{(1+2\langle m\rangle_{ss})}\right\}\\&\left.\times\exp(\lambda_3\tau)_{ss}\right],\end{aligned} \tag{57}$$

where λ_1, λ_2, and λ_3 are given in Eqs. (42) and (43). Its behavior in the weak-driving-field limit is shown in Fig. 9 for several different values of the squeezing parameter r. It can be seen that the correlation function vanishes at zero delay $[g^{(2)}(0)=0]$ for all values of r indicating that the probability of detecting two photons simultaneously remains zero. Fluorescent light is thus always antibunched. This is a reflection of the fact that a two-level atom cannot emit two or more photons simultaneously. After each emission the atom returns to the ground state. It must be excited before another emission can take place. The effect of the squeezed vacuum is observed, however, in the time dependence. When a

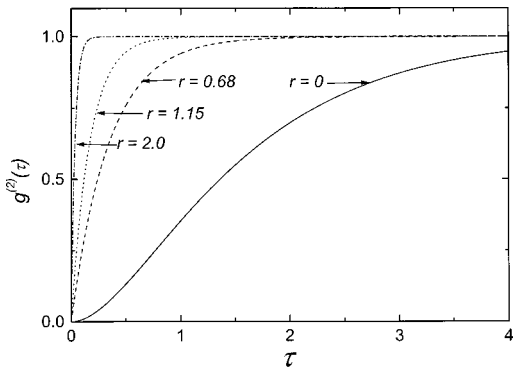

FIG. 9. Second-order intensity correlation function $g^{(2)}(\tau)$ of the fluorescent light below threshold for different values of r, $C=0.4$, $\theta=0$, and $Y=0.1$. $g^{(2)}(0)<1$ reflects the nonclassical effect of antibunching.

squeezed vacuum is introduced, $g^{(2)}(\tau)$ approaches unity at a faster rate than in the case of the ordinary vacuum ($r=0$). This is because the squeezed vacuum enhances the decay of coherence in proportion to the mean photon number $N(r)=\sinh^2(r)$. We also find that in the weak-driving-field limit the phase sensitivity of $g^{(2)}(\tau)$ is negligible.

In the strong-driving-field limit the eigenvalues λ_2 and λ_3 given in Eqs. (42) and (43) become complex and their imaginary part leads to an oscillatory behavior for $g^{(2)}(\tau)$, as it approaches unity with increasing delay τ. For short time delay the behavior is similar to that for the weak driving field. This behavior $g^{(2)}(\tau)$ is shown in Figs. 10(a) and 10(b) for $\theta=0$ and π, respectively. The oscillatory behavior of $g^{(2)}(\tau)$ as a function of τ is due to Rabi oscillations of the atom. The

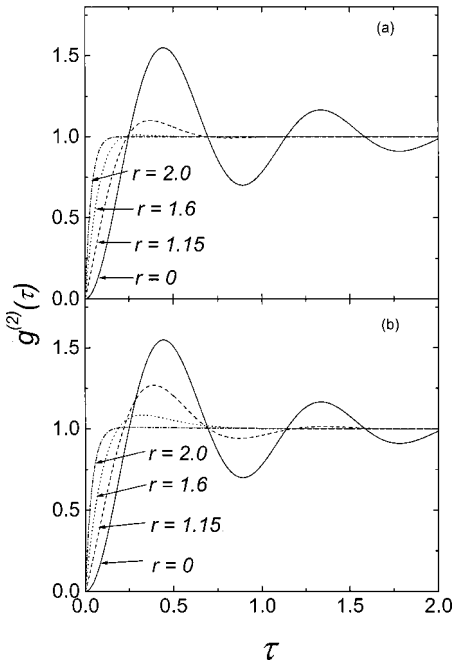

FIG. 10. Second-order intensity correlation function $g^{(2)}(\tau)$ of the fluorescent light above threshold for different values of r, $C=0.4$, $Y=10$, and (a) $\theta=\pi$, (b) $\theta=0$. $g^{(2)}(0)<1$ reflects the nonclassical effect of antibunching.

presence of the squeezed vacuum has an effect on the amplitude of these oscillations for both $\theta=0$ and π. The amplitude decreases as squeezing increases and eventually the oscillations are washed out for sufficiently large values of squeezing. This behavior is more pronounced when the driving field and squeezed vacuum are out of phase than when they are in phase. We observe a similar damping of oscillatory behavior when the squeezed vacuum is replaced by thermal light ($|M|=0$). Thus the decrease in the amplitude of the oscillation is due to the mean photon number of the mode that is coupled to the atom. This behavior is qualitatively similar to that reported by Rice and Baird [12] for a single two-level atom inside a coherently driven cavity with injected squeezed vacuum although it differs quantitatively.

VII. CONCLUSIONS

We have derived a generalized Fokker-Planck equation without using the system-size expansion or any truncation for a single two-level atom placed inside a coherently driven cavity when the atom is coupled to a broadband squeezed vacuum. Our results include atomic and cavity detunings and also atomic and cavity decays. Using this Fokker-Planck equation we have studied atomic inversion, the fluorescent spectrum, and the second-order intensity correlation function of the transmitted and fluorescent light in the bad-cavity limit. For $r=0$ our results reduce to those for an atom decaying to the ordinary vacuum [14].

Mean atomic inversion, in general, increases with increasing mean photon number of the squeezed reservoir. This behavior, however, shows phase sensitivity. For example, when $\theta=\pi$ and the cavity mode and the driving field are equally detuned with respect to the atomic transition frequency, the atomic inversion shows a dip as a function of the detuning due to destructive interference between the driving field and the squeezed vacuum. As a function of detuning the atomic inversion shows two peaks located symmetrically at nonzero detunings. The presence of the squeezed reservoir effectively reduces the threshold value of C for seeing the vacuum Rabi splitting. Such phase sensitivity is not seen when the atom is coupled to a thermal reservoir.

When the atom is coupled to the ordinary vacuum, then, on resonance, photon antibunching in the transmitted light can be observed only for weak driving fields ($Y\ll 1$) and small values of the cooperativity parameter ($C<1/\sqrt{2}$). It is possible to see antibunching for a large value of C at nonzero detunings. Antibunching in all these cases can be explained in terms of self-homodyning between coherent and incoherent component of the intracavity field. The major contributions to the antibunching for $r=0$ are due to squeezing in the quadrature $\hat{A}_1$ which is in phase with the driving field. When the ordinary vacuum coupled to the atom is replaced by a squeezed vacuum and the squeezing parameter is small, we find that antibunching decreases and transmitted light can become bunched. This is because squeezing in the quadrature $\hat{A}_1$ decreases. With further increase in r we find that $g^{(2)}(0)$ decreases and the transmitted light becomes antibunched. Antibunching for large r is due to a reduction in the intensity fluctuation of the incoherent component.

In the weak-driving-field limit we find a narrowing of the spectrum with increasing degree of squeezing. In this limit the spectrum and the second-order intensity correlation function are not strongly phase sensitive. The effect of a squeezed vacuum on $g^{(2)}(\tau)$ is to enhance the rate of its decay. This is due to the increase of the dephasing of the Rabi oscillation with increasing r. In the strong-driving-field limit we find phase sensitive behavior for both the spectrum and the second-order intensity correlation function. In this limit the overall effect of the squeezed vacuum is to increase the width of the spectrum and damp out the amplitude of oscillations in the second-order intensity correlation function. The widths of the Mollow triplets increase as the degree of squeezing increases when $\theta=0$. On the other hand, for $\theta=\pi$, the sidebands are broadened whereas the central peak becomes narrower. For the second-order intensity correlation function the amplitude of oscillations damps out faster for $\theta=\pi$ than for $\theta=0$ as the degree of squeezing increases.

ACKNOWLEDGMENTS

The authors would like to thank Dr. Surendra Singh for many helpful discussions. This work was supported in part by the Office of Naval Research and the Arkansas Science and Technology Authority. D.E. acknowledges support from the ICSC World Laboratory.

[1] R.E. Slusher, L.W. Hollberg, B. Yurke, J.C. Mertz, and J.F. Valley, Phys. Rev. Lett. **55**, 2409 (1985).
[2] M.W. Maede, P. Kumar, and J. Shapiro, Opt. Lett. **12**, 161 (1987).
[3] R.M. Shelby, M.D. Levenson, S.H. Perlmutter, R.G. De Voe, and D.F. Walls, Phys. Rev. Lett. **57**, 691 (1986).
[4] L.A. Wu, H.J. Kimble, J.L. Hall, and H. Wu, Phys. Rev. Lett. **57**, 2520 (1986).
[5] C.W. Gardiner, Phys. Rev. Lett. **56**, 1917 (1986).
[6] H.J. Carmichael, A.S. Lane, and D.F. Walls, Phys. Rev. Lett. **58**, 2539 (1987); J. Mod. Opt. **34**, 821 (1987).
[7] B.N. Jagatap and S.V. Lawande, Phys. Rev. A **44**, 6030 (1991).
[8] R. Vyas and S. Singh, Phys. Rev. A **45**, 8095 (1992).
[9] I.E. Lyublinskaya and R. Vyas, Phys. Rev. A **48**, 3966 (1993).
[10] A.S. Parkins and C.W. Gardiner, Phys. Rev. A **40**, 3796 (1989).
[11] P.R. Rice and L.M. Pedrotti, J. Opt. Soc. Am. B **9**, 2008 (1992).
[12] P.R. Rice and C.A. Baird, Phys. Rev. A **53**, 3633 (1996).
[13] B.J. Dalton, Z. Ficek, and S. Swain, J. Mod. Opt. **46**, 379 (1999).
[14] C. Wang and R. Vyas, Phys. Rev. A **51**, 2516 (1995).
[15] C. Wang and R. Vyas, Phys. Rev. A **55**, 823 (1997).
[16] C. Wang and R. Vyas, Phys. Rev. A **54**, 4453 (1996).
[17] J.P. Gordon, Phys. Rev. **161**, 367 (1967).